1040-5488/15/9212-1170/0 VOL. 92, NO. 12, PP. 1170–1181
OPTOMETRY AND VISION SCIENCE

ORIGINAL ARTICLE

Distortion Correction of Visante Optical Coherence Tomography Cornea Images

Viswanathan Ramasubramanian* and Adrian Glasser*

ABSTRACT

Purpose. Quantitative biometry measurements from uncorrected anterior segment optical coherence tomography (AS-OCT) images are inaccurate because of spatial and optical distortions. Prior reported distortion correction equations for the Visante AS-OCT were not reproducible. The goal was to calculate the distortions and provide equations to correct corneal parameters for the Visante AS-OCT to get a central corneal radius of curvature from young and older subjects.

Methods. Five contact lenses (CLs) of known front and back radii of curvature and central thickness were imaged using the Visante AS-OCT (Carl Zeiss, Dublin, CA). Contact lens surface coordinates from Visante images were identified and fitted with a circle using custom Matlab image analysis software. Spatial and optical distortions of the Visante image of the CL radii of curvature and thickness were calculated and corrected. Visante images were also captured from 24 younger (aged 21 to 36 years) and 30 older (aged 36 to 48 years) human subjects. Corneal radii of curvature and thickness measurements from these subjects were corrected, and intrasession and intersession repeatabilities of the corneal parameters were calculated.

Results. Root mean square error of radius and power of the CL surfaces after distortion correction were 0.02 mm and 0.18D for the front and 0.011 mm and 0.11D for the back, respectively. Intraclass correlation coefficient for intrasession and intersession repeatability for all the corneal parameters from the human subjects was greater than 0.88 in both age groups.

Conclusions. A distortion correction algorithm was developed for the Visante AS-OCT and applied to extract human corneal radius of curvature measurements.

(Optom Vis Sci 2015;92:1170–1181)

Key Words: Visante AS-OCT, spatial distortion, optical distortion, contact lenses, image analysis, intraclass correlation coefficient

Accurate measurement of corneal anterior and posterior radii of curvature and thickness is useful for contact lens (CL) fitting, refractive surgeries, diagnosis, and management of corneal disorders and optical modeling. Various imaging modalities such as Scheimpflug photography,[1–3] scanning slit topography,[4–6] ultrasound biomicroscopy,[7,8] and anterior segment optical coherence tomography (AS-OCT)[9–11] have been used to measure corneal shape and thickness.

The purpose of the current study was to get central corneal radius of curvature and central thickness measurements of sufficient accuracy to perform paraxial schematic eye calculations to try to calculate refraction and accommodation on a series of eyes in which the rest of the anterior segment biometry parameters were measured with ultrasound biomicroscopy (UBM).[12–14] Because of the low resolution of UBM, it was not possible to get corneal curvature measurement from the UBM measurements. Hence, Visante, a commercial AS-OCT instrument with an axial resolution of 18 μm,[15] was chosen to perform noninvasive measurement of anterior segment parameters.

Prior studies have reported spatial (geometric) and optical (refractive) distortions in custom-built OCT systems.[16–19] The spatial distortions may be caused by the nonlinear axial scanning and nontelecentric lateral scanning architecture.[16] Optical distortions of optical surfaces occur because of the refractive effects of a surface preceding the surface of interest. Spatial and optical distortions have been reported in Visante AS-OCT images,[20] although the exact source of the spatial distortion is unknown. Kao et al[21] reported no spatial distortion in the Visante image of an optical flat captured using "Enhanced High-Resolution Corneal Mode." However, that mode captures a magnified image of a small area that may not be enough to accurately determine the presence of distortion. The instrument manufacturer does not provide information about the correction applied to the images in various scan modes. The presence of residual errors in corneal and anterior segment parameters measured in a calibrated model eye using the

*PhD

College of Optometry, University of Houston, Houston, Texas (both authors).

Supplemental digital content is available for this article. Direct URL citations appear in the printed text and are provided in the HTML and PDF versions of this article on the journal's Web site (www.optvissci.com).

built-in Visante software[20] suggests that the Visante software does not provide robust spatial and optical distortion correction.

Dunne et al.[20] previously described a distortion correction for the Visante AS-OCT (version 1.0.12.1896). When the anterior corneal surface distortion correction equation from that article was used to try to correct calibration surfaces (rigid custom-made CLs) imaged from another Visante instrument (version 2.0.1.88), it did not yield correct values. There are a number of uncertainties in the description of that prior work: it is not clear whether raw or Visante distortion-corrected images were used for their analysis; the Visante software described in that study appears to have capabilities that are not available in subsequent versions, suggesting substantial differences between versions; there is some confusion over what is considered as the image x and y axes in the prior study, for example, x coordinates are described in a vertical line of pixels. Because the software versions are different, it is possible that the Visante software has been modified, so that the method described previously may not be applicable to later software versions.

For these reasons, this current study was undertaken to a) use custom-fabricated CLs of known parameters to measure spatial and optical distortions and provide equations to obtain corrected corneal parameters from Visante AS-OCT images, b) apply the distortion correction to corneal parameters measured from Visante AS-OCT images captured in 24 younger and 30 older human subjects, and c) obtain corneal front and back surface radii of curvatures and central corneal thickness measurements from younger and older human subjects that are of sufficient accuracy to use those values in future schematic eye calculations.

MATERIALS AND METHODS

Visante AS-OCT (Carl Zeiss, Dublin, CA) (version 2.0.1.88) images were captured using the ''anterior segment single'' mode or the ''raw image'' mode. When a Visante image is captured and saved, the Visante software automatically stores a raw unprocessed image in DICOM format in the folders created by the Visante software with 41 seemingly random character file names. These files can be located by exiting the Visante software and searching the hard drive for files created by time and date or by searching for files with the extension ''.EX.DCM.'' These images were exported to a USB drive and converted to bitmap (.bmp) format using a custom-developed Matlab (MathWorks, Natick, MA) program. Raw images from the Visante ''anterior segment single'' mode and the ''raw image'' mode were shown to be identical by image subtraction that yielded pixel values of only zeros. The Visante software applies no overlay or distortion correction to these images. All further processing described here was performed on these raw AS-OCT images.

Spatial Calibration

The horizontal spatial pixel to millimeter conversion factor was calculated by imaging a millimeter-scaled ruler placed perpendicular to the instrument measurement axis. The ruler was positioned at five different axial distances along the instrument optical measurement axis. This resulted in the ruler being imaged at five different vertical (y axis) positions in the AS-OCT images in five separate images. The millimeter markings in each image were manually marked using a custom-developed Matlab program (Fig. 1A). The horizontal pixel to millimeter conversion factor was similar for all five vertical positions of the ruler on the image. The mean ± SD of horizontal pixel to millimeter conversion factor from 15 measurements in the five images was 31.80 ± 0.50 pixels/mm. The low SD obtained from repeated measures indicates the accuracy of the manual markings and the absence of significant variations in the calibration procedure. This horizontal calibration is therefore applicable at any vertical position in the image.

To determine the vertical spatial pixel to millimeter conversion factor, a microscope slide and independently a thinner coverslip were fixed to a micrometer translation stage on a goniometer (Fig. 1B). The goniometer was adjusted so that the surface of the microscopic slide/coverslip was perpendicular to the instrument optical measurement axis. The micrometer translation stage was used to move the slide/coverslip in 0.5-mm steps (a total of 15 positions) along the instrument measurement axis, and images were captured at each position. The position of the front and back surface of the slide/coverslip on the image was manually marked at three different horizontal locations in the images (left, middle, and right) (Fig. 1C). The difference in the vertical position between the corresponding red points in each successive image gave the number of pixels moved in the image for 0.5-mm movement in real space. The vertical pixel to millimeter conversion factor was similar for the 15 axial positions of the slide and the coverslip in the image. The mean ± SD of vertical spatial pixel to millimeter conversion factor from 168 measurements [six locations on each image × 14 measurements between successive images × 2 (slide and the coverslip)] was 25.77 ± 1.09 pixels/mm.

To calculate the spatial and optical distortion correction factors, five polymethylmethacrylate (PMMA) CLs of known spherical surface curvatures and vertex thickness were imaged with the Visante. The vertices of the CLs were aligned with the optical axis of the Visante, and this was ensured by the appearance of the bright streak of light reflecting off the vertex of the surface being measured. This approach to imaging surfaces is per the manufacturer's operating procedure. The PMMA CLs were custom-cut on a lathe (DAC International, CA), and the radii of curvature of the CL surfaces were verified using a radiuscope. The precision of the radiuscope to measure the radii of curvature of the PMMA CLs was 0.01 mm. The parameters of the CLs used are listed in Table 1. For the analysis of the Visante images, the front and back surfaces of the CLs were identified in the images using a custom-developed automated Matlab image analysis program. Both front and back surface points corresponding to a central 8-mm diameter were fit with circles (Fig. 1D). Later (see below), the same analysis methods were also applied to human corneas. Visante AS-OCT images of human eyes with the central 8-mm anterior and posterior corneal surfaces digitized were also well fitted with a circle (Fig. 1E). A circle provided acceptable fits to the central 8 mm of the CL and the corneal surface points as judged by evidence of no systematic pattern to the residuals and was used for calculating distortion corrections.

Front Surface Distortion Correction

To correct the spatial distortion of the front CL surface, the identified surface coordinates and the fitted circle coordinates

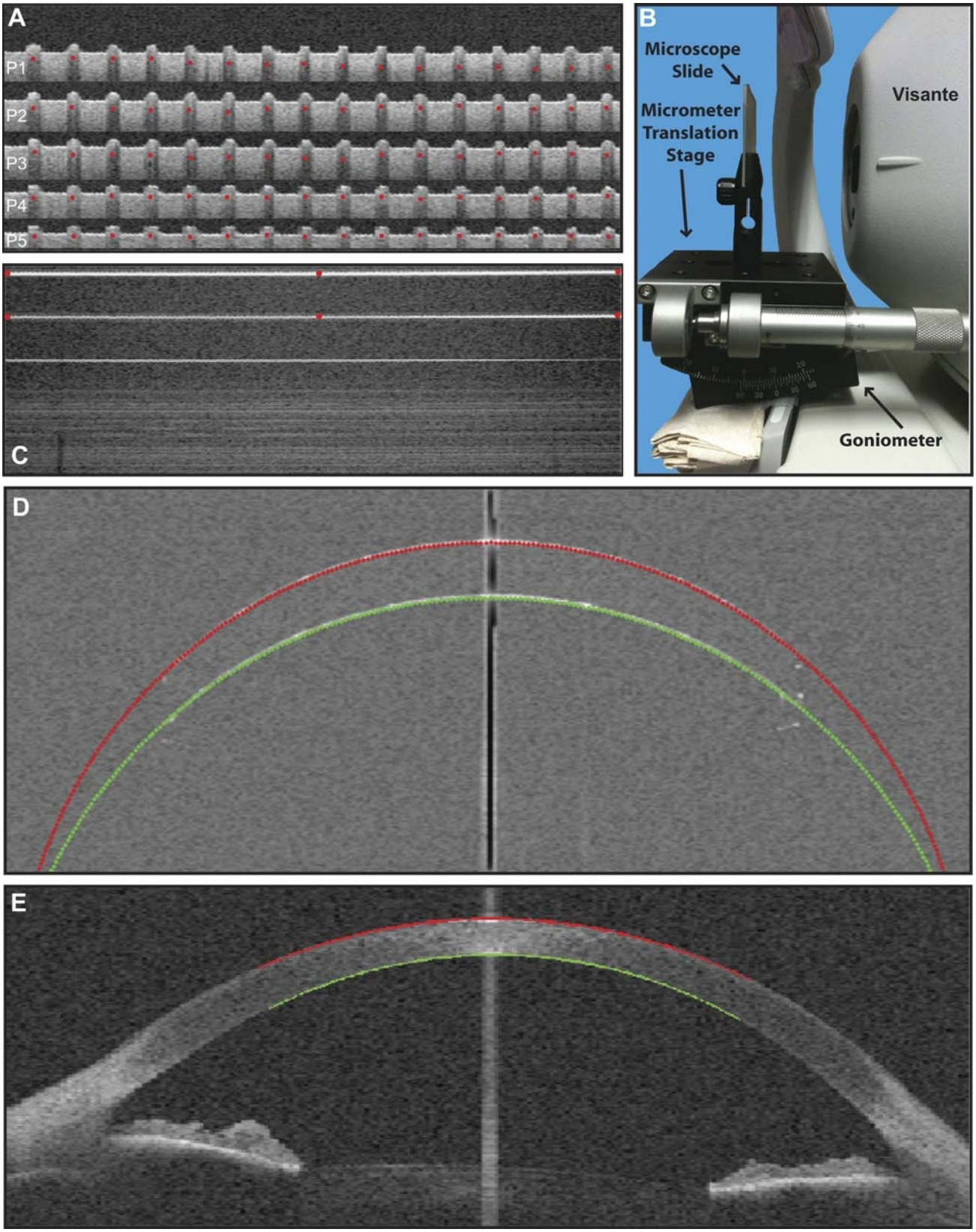

FIGURE 1.

(A) An overlay of five Visante images of a ruler at five different vertical positions (P1 to P5) with red points marked on the millimeter gradations to calculate the horizontal pixel to millimeter conversion factor. (B) Experimental setup to determine the vertical pixel to millimeter conversion factor. (C) Visante image of a microscope slide at one axial position with red points marked on the front and back slide surfaces. The third horizontal line is an artifact or ''shadow'' resulting from the AS-OCT imaging of a glass slide. (D) Raw Visante image of a CL with circles fitted to the central 8 mm of the front (red) and back (green) surface. (E) Raw Visante image from a single subject showing circle fits to the central 8 mm of the anterior (red) and posterior (green) corneal surface. A color version of this figure is available online at www.optvissci.com.

TABLE 1.
Parameters of the spherical calibration CLs used

CLs	Actual parameters		
	Front surface radius of curvature, mm	Central thickness, mm	Back surface radius of curvature, mm
CL 01	6.60	0.80	6.30
CL 02	7.30	0.80	7.00
CL 03	7.55	0.80	7.25
CL 04	7.80	0.80	7.50
CL 05	8.30	0.80	8.00

were converted from pixels to millimeters using the x and y spatial calibration factors described above. If necessary, the calibrated coordinates were rotated to achieve mirror symmetry about the vertex to correct for any tilt of the CL in the AS-OCT image. The coordinates of the fitted circle (the distorted circle) were scaled and cropped such that the vertex of the surface was set to $x = 0$, $y = 0$ and the range of x data spanned from -4 to +4 mm (for the central 8-mm diameter). The radius of curvature of the circle fitted to these data provided a spatially distorted front CL radius of curvature. Coordinates were then generated in Matlab for a circle with a radius that corresponded to the actual CL front surface radius of curvature (the actual circle). These generated coordinates used the same matching relative x coordinates as obtained from the CL surface in the distorted image. These two curves are shown in Fig. 2A. A two-step process was then used to correct the spatial distortions. In the first step, the AS-OCT image spatial distortion was calculated by dividing each y coordinate value of the actual circle by each corresponding y coordinate value from the distorted circle. Fig. 2B shows a plot of the calculated spatial distortion as a function of x coordinates from one CL. The calibration curve was then fitted with a sixth-order polynomial that provided the spatial distortion correction equation for this CL. A sixth-order polynomial was the smallest polynomial order that provided the best fit with r^2 of 1 and residuals close to 0. Although the coefficients of polynomials (Table 2) greater than second order seem small and negligible, using a second-order polynomial alone yielded radii that did not match the actual radii of the CL surfaces. The coefficients for each term from five sixth-order equations (Table 2) from the five separate CLs were averaged to generate a mean distortion correction equation. This mean distortion correction equation was applied to each front CL surface y coordinate value to correct the spatial distortion (step 1). Panels C and D of Fig. 2 show a comparison of actual and measured front CL surface radii of curvature for the five CLs before and after the initial distortion correction (step 1). As can be seen from the resulting curve (Fig. 2D), the data points did not lie exactly on the expected 1:1 line, which would demonstrate complete correction. A second step in the distortion correction was then required. In the second step, the data points from all the calibration CL surfaces were then fitted with a second-order polynomial equation as shown in Fig. 2D. This polynomial equation was then applied (step 2) to the distortion-corrected radius of each surface from step 1. Fig. 2E shows that, after applying step 2, the distortion-corrected radii fall on the 1:1 line with a slope close to 1. Bland-Altman plots show a maximum difference of less than 50 μm between the actual and final distortion-corrected front surface radii of curvatures (Fig. 2F).

Thickness Optical Correction

In the OCT image, the back surface of the CL is the *image* of the actual back surface as viewed refracted by the CL. The thickness of this central CL *image* was measured from the AS-OCT images as the distance between the front and back CL surfaces at the vertex. There is no spatial distortion to the CL thickness at the vertex because the CL vertex corresponds to the optical axis of the OCT instrument. The axial thickness observed in the AS-OCT image is the apparent thickness of the CL, which is affected optically by refraction at the front surface and by the CL refractive index. The actual thickness of the CL can be calculated from the OCT image using simple paraxial optics. Refractive index of PMMA for the AS-OCT wavelength of 1310 nm was calculated to be 1.4738.[22] Equations 1 through 4 were used to correct the optical distortions for the central CL thickness. First, the front CL surface power was calculated:

$$F = \frac{1000 \times (n_{PMMA} - n_{air})}{r_{fs}} \quad (1)$$

where F is surface power (in diopters) of front CL surface; n_{PMMA} is refractive index of PMMA at a wavelength of 1310 nm; n_{air}, the refractive index of air is 1.00; and r_{fs} is the actual front surface radius of curvature (in millimeters) calculated as described above. Next, the vergence to the CL image posterior surface after refraction by the CL front surface was calculated:

$$L' = \frac{1000 \times n_{PMMA}}{l'} \quad (2)$$

where L' is image vergence (in diopters), l' is image distance in millimeters (measured CL image thickness from OCT image). Next, the vergence before refraction by the CL front surface of the actual CL posterior surface was calculated:

$$L = L' - F \quad (3)$$

where L is object vergence (in diopters). Finally, the distance before refraction by the CL front surface to the actual CL posterior surface was calculated:

$$l = \frac{1000 \times n_{air}}{L} \quad (4)$$

where l is object distance or the optically corrected (i.e., true) central CL thickness (in millimeters).

Back Surface Spatial and Optical Correction

The CL back surface as seen in the AS-OCT image is the *image* of the actual CL back surface refracted by the front CL surface and has both the optical distortion from being refracted by the CL front surface and the CL thickness, and it has the spatial distortion from the AS-OCT instrument. The process for determining the spatial distortion of this surface is to a) generate the *image* of the actual CL back surface as though seen through the CL and b) to fit that image with a circle and then to compare that fitted circle with the CL back surface from the OCT image.

To generate the *image* of the actual CL back surface (i.e., the target back CL surface) as refracted through the CL front surface, the position of the center of curvature and the radius of the target CL back surface has to be calculated. The center of curvature of the actual CL back surface is the *object* for the CL front surface. Therefore, the object distance is the CL thickness plus the distance

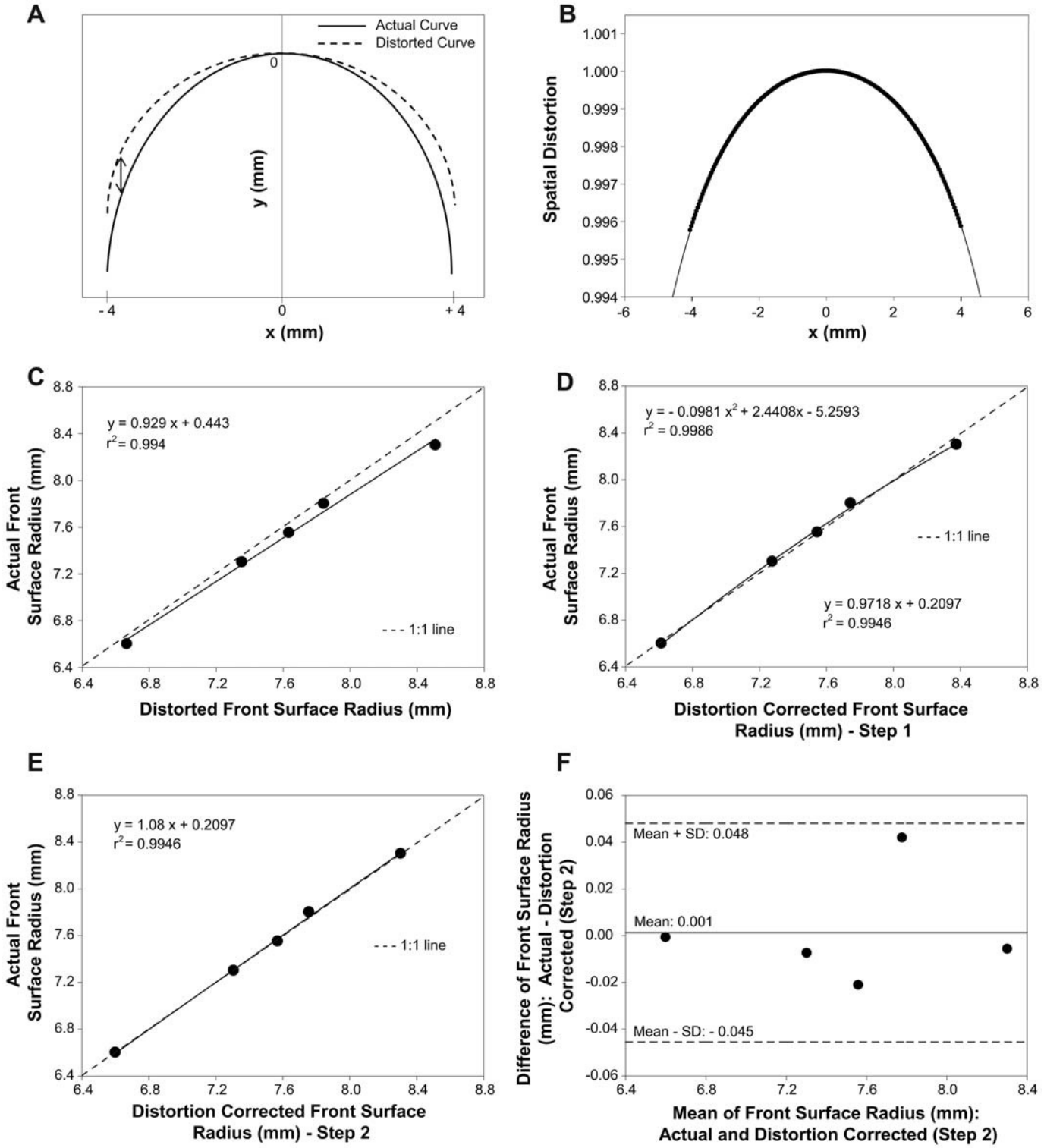

FIGURE 2.

(A) Illustration showing the calculation of spatial distortion from the actual (solid black) and distorted (dashed black) curves. (B) Calibration curve of the front surface of a CL (CL 05) with a sixth-order polynomial fit. The equation of this polynomial is: Spatial Distortion = $-7.8086e^{-8} \times x^6 + 7.3596e^{-10} \times x^5 - 2.7542e^{-6} \times x^4 - 1.0987e^{-8} \times x^3 - 1.7667e^{-4} \times x^2 + 3.0205e^{-8} \times x + 1.00$. (C) Comparison of the actual and distorted front surface radii of curvature from all five CLs. (D) Step 1: Comparison of the actual and distortion corrected front surface radii of curvature after applying the average sixth-order polynomial. (E) Step 2: Comparison of the distortion-corrected front surface radii of curvature after applying the second polynomial correction. (F) Bland-Altman comparison between actual and distortion-corrected front surface radii of curvature after step 2.

TABLE 2.
Spatial distortion correction equations calculated for the front and back surfaces for all CLs

		Coefficients of the spatial distortion correction equation						
CLs	Surfaces	x^6	x^5	x^4	x^3	x^2	x	Constant
CL 01	Front	−1.9085E-07	−2.3894E-09	−2.0168E-06	3.5548E-08	−1.1906E-04	−9.7671E-08	1.000
CL 02		−6.5333E-08	7.1828E-10	−1.2742E-06	−1.0653E-08	−7.1063E-05	2.9139E-08	1.000
CL 03		−7.4584E-08	−4.1367E-19	−1.7218E-06	−2.3123E-18	−9.8337E-05	4.9935E-17	1.000
CL 04		−2.9999E-08	3.0496E-10	−7.8856E-07	−4.5272E-09	−4.6100E-05	1.2386E-08	1.000
CL 05		−7.8086E-08	7.3596E-10	−2.7542E-06	−1.0987E-08	−1.7667E-04	3.0205E-08	1.000
Mean		−8.7770E-08	−1.2605E-10	−1.7111E-06	1.8761E-09	−1.0224E-04	−5.1882E-09	1.000
SD		6.0691E-08	1.3020E-09	7.4559E-07	1.9370E-08	4.9902E-05	5.3197E-08	6.8719E-07
		x^6	x^5	x^4	x^3	x^2	x	Constant
CL 01	Back	−1.8615E-06	−1.6229E-19	−1.8868E-05	1.1335E-17	−1.1326E-03	−1.4132E-16	1.000
CL 02		−7.8553E-07	−9.3164E-21	−1.5311E-05	1.0225E-17	−8.5766E-04	−1.1615E-16	1.000
CL 03		−5.8190E-07	6.4211E-09	−1.3176E-05	−9.5732E-08	−7.5250E-04	2.6305E-07	1.000
CL 04		−4.4478E-07	1.3909E-08	−1.1669E-05	−2.0696E-07	−6.8510E-04	5.6751E-07	1.000
CL 05		−2.9919E-07	1.8331E-18	−1.0472E-05	−2.5513E-17	−6.6796E-04	1.3157E-17	1.000
Mean		−7.9458E-07	4.0659E-09	−1.3899E-05	−6.0539E-08	−8.1917E-04	1.6611E-07	1.000
SD		6.2279E-07	6.1648E-09	3.3136E-06	9.1752E-08	1.9040E-04	2.5164E-07	7.1063E-06

to the back surface center of curvature. The object vergence (L_1) is then given by:

$$L_1 = \frac{1000 \times n_{PMMA}}{r_{bs} + CT_{actual}} \quad (5)$$

where r_{bs} is actual (i.e., true, known) CL back surface radius of curvature (in millimeters), and CT_{actual} is actual CL center thickness (in millimeters). The denominator (r_{bs} + CT_{actual}) represents the object distance (distance of the actual CL back surface center of curvature from the CL front surface).

After refraction by the CL front surface, the image vergence L'_1 to the center of curvature of the target CL back surface is:

$$L'_1 = L_1 + F \quad (6)$$

where F is the power of the front CL surface (in diopters) from equation 1.

The image distance (l'_1) that is the distance of the target CL back surface center of curvature from the CL front surface is:

$$l'_1 = \frac{1000 \times n_{air}}{L'_1} \quad (7)$$

The target radius of curvature can then be obtained by subtracting the thickness of the CL OCT image as:

$$r_{tbs} = l'_1 - CT_{OCT} \quad (8)$$

where r_{tbs} is the target CL back surface radius of curvature (in millimeters), and CT_{OCT} is the central CL thickness (in millimeters) measured from the AS-OCT image.

Once the target back CL surface radius (r_{tbs}) is known, this can be directly compared with the back CL surface from the AS-OCT image and the spatial distortion can be calculated using the methods described above for the CL front surface. The CL back surface coordinates were extracted from the AS-OCT images for the central 8-mm diameter and fitted with a circle (this being the distorted circle). The radius of curvature calculated from the distorted circle is the spatially and optically distorted back CL radius. The target back CL surface radius was then used to generate a target circle x and y coordinates in Matlab using the same x axis coordinates as were extracted from the AS-OCT image. The vertices of the target circle and the distorted circle were set to $x = 0$, $y = 0$, and the data were rotated, if necessary, and scaled and cropped from −4 to +4 mm as described above. The ratio of y coordinate positions for each corresponding x coordinate position was calculated to generate a sixth-order distortion correction polynomial for each CL (Table 2). Five polynomials from the five CLs were averaged to generate a mean distortion correction equation for the CL back surface. This mean distortion correction equation was applied to each CL back surface y coordinate value to correct the spatial distortion (step 1). Panels A and B of Fig. 3 show a comparison of target back surface radii (r_{tbs}) and measured back surface radii of curvature for the five CLs before and after the distortion correction, respectively (step 1). The spatial distortion for the back surface also required a second correction step similar to that used on the front surface. Data points for the individual CLs in Fig. 3B were fitted with a second-order polynomial. This polynomial was applied (step 2) to the distortion-corrected radius for each CL surface calculated in step 1 to get the spatial distortion–corrected back surface radius (r'_{tbs}) closer to target back surface radius (r_{tbs}) (Fig. 3C). Bland-Altman plots show that the maximum difference between r_{tbs} and r'_{tbs} is less than 40 μm (Fig. 3D).

To get an optically corrected CL back surface radius (r_{cbs}) from the spatial distortion–corrected CL back surface radius (r_{tbs}), the position of the center of curvature of the corrected CL back surface has to be calculated. To do this, this spatially corrected surface must again be optically transformed by refraction through the CL front surface. The center of curvature of the spatially corrected surface serves as the object for the CL front surface, and then the object vergence to the CL front surface can be calculated:

$$L_2 = \frac{1000 \times n_{air}}{r'_{tbs} + CT_{OCT}} \quad (9)$$

where L_2 is the object vergence for the center of the curvature of the spatial distortion–corrected back CL surface, (r'_{tbs} + CT_{OCT})

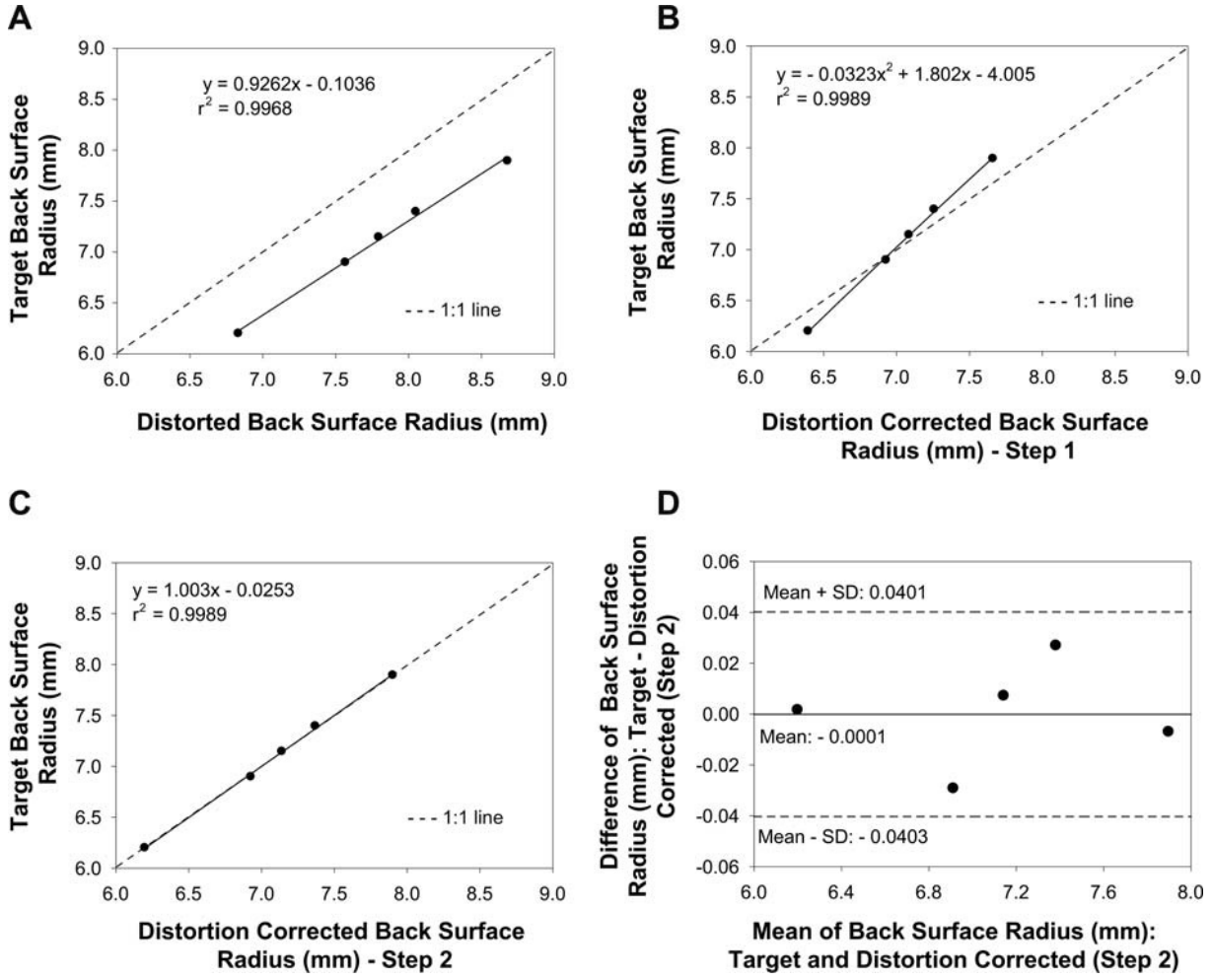

FIGURE 3.

(A) Comparison of the target and distorted back surface radii of curvature from all five CLs. (B) Step 1: Comparison of the target and distortion-corrected back surface radii of curvature after applying the average sixth-order polynomial. (C) Step 2: Comparison of the distortion-corrected back surface radii of curvature after applying the second polynomial correction. (D) Bland-Altman comparison between target and distortion-corrected back surface radii of curvature after step 2.

represents the object distance (distance of the spatial distortion–corrected back CL surface center of curvature from the front CL surface).

The image vergence (L'_2) at the center of the curvature of the optically corrected back CL surface is:

$$L'_2 = L_2 + F \tag{10}$$

where F is the power of the front CL surface (in diopters) from equation 1.

The image distance (l'_2) is the distance of the optically corrected back CL surface center of curvature from the front CL surface and is calculated from:

$$l'_2 = \frac{1000 \times n_{PMMA}}{L'_2} \tag{11}$$

Finally, the optically corrected CL back surface radius of curvature can be calculated from:

$$r_{cbs} = l'_2 - Corrected\,CT \tag{12}$$

where r_{cbs} is the optically corrected back CL surface radius of curvature (in millimeters), and *Corrected CT* is the optically corrected center CL thickness (l) calculated from equation 4.

TABLE 3.

RMS error of radius and power at various steps in the distortion correction process

Measured parameters	RMS error of radius/power		
	Before distortion correction, mm/D	After spatial distortion correction, mm/D	After optical distortion correction, mm/D
Front CLs surface radius	0.11/0.86	0.02/0.18	NA
Back CLs surface radius	0.58/5.12	0.21/1.82	0.011/0.110
Central CLs thickness	0.364/NA	NA	0.004/NA

RMS error for the measured front and back CL radii and central CL thickness in units of millimeters and diopters compared with known values.

NA, not applicable.

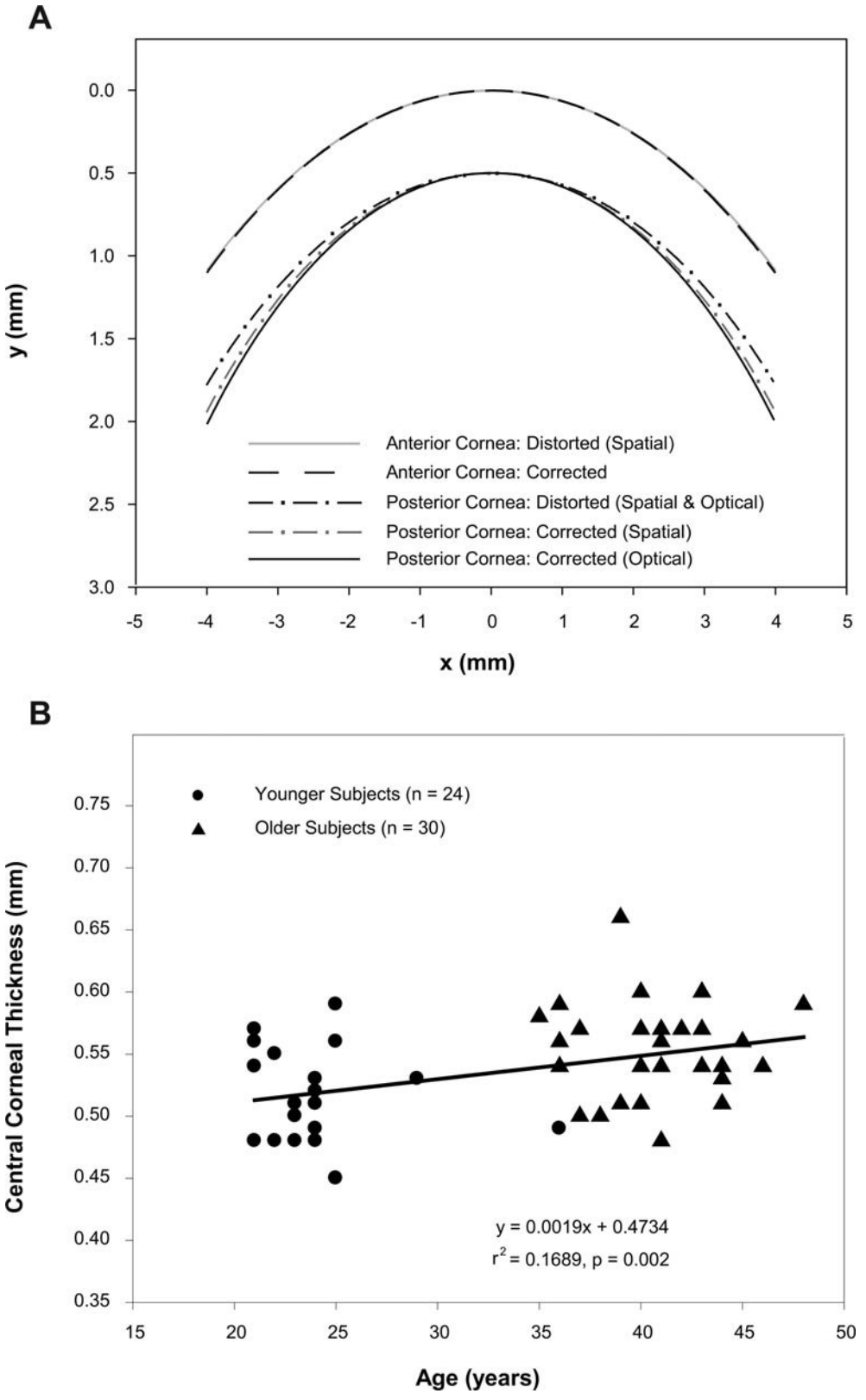

FIGURE 4.

(A) Comparison of the anterior and posterior corneal surface (central 8-mm diameter) before and after spatial distortion correction using equations listed in the Appendix for a single subject. (B) Graph of the measured central corneal thickness as a function of age.

Subjects

To use and test these optical and spatial corrections on corneal OCT images, two Visante images of the horizontal meridian of the anterior segment were captured from 24 younger subjects (seven men and 17 women), aged 21 to 36 years (mean ± SD, 24.04 ± 3.10 years) and 30 older subjects (10 men and 20 women), aged 36 to 48 years (mean ± SD, 40.83 ± 3.25 years) with normal visual and ocular histories. The study followed the tenets of the Declaration of Helsinki and was performed in accordance with an institutionally approved human subject protocol. To assess the intrasession and intersession repeatability, 15 younger subjects and three older subjects had AS-OCT scans repeated twice on a different day at least 5 days apart. Repeatability analysis was performed in SPSS software (version 20; SPSS Inc., Chicago, IL). Anterior and posterior corneal surface coordinates were identified and extracted using a custom Matlab image analysis program. The corneal surface coordinates were converted from pixels to millimeters using the calibration factors described previously. Central corneal thickness was measured as the vertical distance between the anterior and posterior corneal surfaces at the vertex. Optical and spatial distortions in the measured corneal parameters were corrected as described above using equations listed in the Appendix (available at http://links.lww.com/OPX/A224).

RESULTS

Root mean square (RMS) errors (millimeters and diopters) of the measured CL front and back radii of curvature and CL thickness at each step of distortion correction compared with known values are shown in Table 3. The power of the front CL surface was calculated using the equation:

$$Front\,CL\,Power\,(D) = \frac{1000 \times (n_k - n_{air})}{Front\,CL\,radius\ of\ curvature\,(mm)} \quad (13)$$

The power of the back CL surface was calculated using the equation:

$$Back\,\mathrm{CL}\,Power\,(\mathrm{D}) = \frac{1000 \times (n_{air} - n_k)}{Back\,CL\,radius\ of\ curvature\,(mm)} \quad (14)$$

where n_k is the refractive index of PMMA at 555 nm (1.493). The RMS error of power for the CL front and back surfaces after full optical and spatial distortion corrections were 0.18 D and 0.11 D, respectively. The mean RMS error of central CL thickness after optical distortion correction was 0.004 mm. Fig. 4A shows the spatially distorted and corrected circle coordinates for the anterior and posterior corneal surfaces from a single subject.

Mean, SD, median, maximum, and minimum values of the measured corneal radii and central thickness from the two subject groups are listed in Table 4. Corneal surface radii of curvature and central thickness values were normally distributed in both subject groups based on the Shapiro-Wilk test ($p > 0.05$). There was a statistically significant difference between mean posterior corneal radius of curvature ($t = -2.035$, $p = 0.048$, independent sample t-test) and mean central corneal thickness ($t = -3.863$, $p < 0.0001$, independent sample t-test) between the two subject groups. Fig. 4B shows the increase in central corneal thickness with age from this group of subjects. There were no statistically significant age-related relationships for either the anterior or the posterior corneal radii of curvature (data not shown).

Intrasession repeatability analysis of the Visante AS-OCT measured anterior and posterior corneal radii of curvature and central corneal thickness was performed for all subjects who had at least two repeats of the AS-OCT scans. Repeatability (intrasession and intersession) was evaluated in terms of a) coefficient of variation, which is the ratio of the SD of the measurements to the mean; b) mean ± SD of the difference between the measurements; and c) intraclass correlation coefficient (ICC). There is a good repeatability for all the three corneal parameters, and the repeatability parameters for intrasession and intersession are comparable (Table 5).

DISCUSSION

This study shows the importance of verifying that measurements from clinical instruments do provide accurate quantitative data and provides an example of the approach that can be undertaken to correct measurements if they are found to be inaccurate. Although prior corrections have been described for Visante OCT images,[20] application of those methods on the Visante OCT raw images failed to yield accurate corrections.

The horizontal pixel to millimeter conversion factor did not vary with distance from the measurement axis of Visante. Hence, there is no spatial distortion in the horizontal plane of the raw Visante image. For the vertical pixel to millimeter conversion

TABLE 4.
Descriptive statistics of the measured corneal parameters for the young and older subject groups

Subjects	Measured parameters	Descriptive statistics, mm				
		Mean	SD	Median	Maximum	Minimum
Young subjects (N = 24)	ARC	7.701	0.275	7.666	8.296	7.218
	PRC	6.528*	0.304	6.486	7.260	6.053
	CT	0.514†	0.035	0.512	0.592	0.454
Older subjects (N = 30)	ARC	7.761	0.213	7.782	8.162	7.234
	PRC	6.679*	0.221	6.708	7.132	6.187
	CT	0.552†	0.036	0.555	0.659	0.483

*†Statistically significant difference between the means ($p < 0.05$, independent sample t-test).
ARC, anterior corneal radius of curvature; PRC, posterior corneal radius of curvature; CT, central corneal thickness.

TABLE 5.
Intrasession and intersession repeatability parameters for various Visante AS-OCT measured parameters

	Intrasession repeatability					
	Young subjects (N = 24)			Older subjects (N = 30)		
Repeatability parameters	ARC	PRC	CT	ARC	PRC	CT
CoV	0.008	0.008	0.019	0.010	0.011	0.020
Mean ± SD difference, mm	0.093 ± 0.082	0.076 ± 0.063	0.014 ± 0.016	0.109 ± 0.084	0.107 ± 0.077	0.015 ± 0.018
ICC	0.952	0.976	0.915	0.899	0.918	0.910
	Intersession repeatability					
	Young subjects (N = 15)			Older subjects (N = 3)		
	ARC	PRC	CT	ARC	PRC	CT
CoV	0.008	0.009	0.023	0.008	0.008	0.035
Mean + SD difference, mm	0.090 ± 0.065	0.084 ± 0.045	0.017 ± 0.018	0.084 ± 0.058	0.071 ± 0.063	0.024 ± 0.022
ICC	0.964	0.980	0.886	0.933	0.969	0.921

ARC, anterior corneal radius of curvature; PRC, posterior corneal radius of curvature; CT, central corneal thickness; CoV, coefficient of variation.

factor, the vertical positions of the microscope slide/coverslip do not change with distortion. Hence, the pixel to millimeter conversion factors calculated from raw Visante images are not affected by distortion and are valid.

The RMS errors for measured power of the CL front and back surfaces corrected for optical and spatial distortions (Table 3) are substantially reduced, and this shows the robustness of the corrections described. The distortion correction equations described are for the central 8-mm diameter only and will not translate to other diameters. These equations are only applicable to the Visante raw images and for the software version 2.0.1.88 and later if no further changes have been made to the optical and distortion corrections by the manufacturer. If Visante "raw images" are truly unprocessed images, then the distortion correction equations described here might work for raw images in later versions of the instrument that do not have hardware changes. The methods described in this article could be used to develop distortion corrections for other AS-OCT systems or software versions.

The population data for corneal parameters (mean and SD) from this study are comparable to data from prior population studies.[23–25] In the current study, the central corneal thickness was found to increase with age (1.9 μm/year). However, several studies report either no change[26–29] or a decreasing trend with age.[30,31] The relationship between corneal thickness and age was reported to be weak[30] or nonsignificant.[26,28] Sample size, ethnicity, age, sex, instrumentation, and analysis methods might contribute to the differences between studies.

Intraclass correlation coefficients for all the measured corneal parameters (intrasession and intersession) were greater than 0.88 in both age groups, which indicates good repeatability. Coefficient of variation and ICC values for corneal thickness were comparable, with similar values from a prior AS-OCT study.[32] Prior studies[33–35] have reported SDs of approximately 5 μm and 10 μm for central corneal thickness and anterior corneal radius of curvature measurements, respectively. The SDs of corneal parameters from the current study are larger than prior studies, and this may be limited by the resolution of the digital OCT images. The purpose of this study was to get as accurate corneal biometry parameters as possible from the OCT images to be used for future paraxial schematic eye calculations. Comparison of Visante-measured corneal biometry parameters after distortion correction with measurements from another instrument or with the built-in Visante pachymetry mode was not performed because it was beyond the scope of this study.

The human cornea is aspheric, and the corneal curvature is flatter in the periphery. However, the Visante OCT image is a digital pixelated image, and the pixel-wise extraction of the corneal boundaries in the original square-pixel OCT image results in corneal digital boundaries that do not resemble the smooth profile of a real corneal surface. In the Visante OCT images, the corneal surfaces at the vertex are represented as straight line segments of about 50 pixels. This is true even out at the periphery of the cornea, but the horizontal line segments of pixels are shorter out at the periphery than they are near the vertex. An attempt was made to fit the corneal surface coordinates with aspheric curves. Because of the pixelated representation of the smooth corneal surface, there is inherent error in fitting either circles or aspheric fits to the corneal boundary pixels. The circle fits were comparable to the aspheric fits over the central 8-mm diameter, and the mean RMS residuals of the circle fits and aspheric fits were similar. This means that there is no material advantage to fitting the pixelated corneal boundaries extracted from the OCT images with aspheric curves. Also, the inherent resolution limitations of the original Visante OCT digital pixelated images mean that it is fundamentally impossible to get anything resembling accurate information regarding corneal asphericity from these images. The same might be said for trying to get a simple radius of curvature from the images, but the distortion correction described in the current study has demonstrated that corneal radius of curvature can be extracted with sufficient accuracy for the purpose previously explained.

The radii of curvature of anterior and posterior corneal surfaces measured in the current study were for the horizontal meridian of the cornea. No prior studies have used Visante OCT to measure the corneal radius of the curvature and to quantify corneal astigmatism. Hence, there is no information available as to the number of meridional measurements required with Visante OCT to accurately quantify corneal astigmatism.

Although the distortion correction applied to the corneal surfaces seems small, clearly, from the CL calibrations (Figs. 2C and 3A), there is a systematic and not insignificant distortion introduced to both the anterior and posterior corneal surfaces that can be corrected to yield a higher degree of accuracy. Distorted corneal radii of curvature and thickness were flatter and thicker than after correction, respectively. If the uncorrected radii and thickness values were used for schematic eye optical calculations, they would make the eye relatively more hyperopic. To calculate the error these distorted values would induce in schematic eye calculations, refractive state of the normally emmetropic Bennetts and Rabbetts schematic eye[36] was calculated using the distorted corneal values. With a distorted anterior corneal radius, the schematic eye was hyperopic, with a refractive error of +1.09D. With a distorted posterior corneal radius, the schematic eye was myopic, with a refractive error of -0.25D. With a distorted corneal thickness, the schematic eye was myopic, with a refractive error of -0.04D. With all the distorted radii and thickness values used together, the schematic eye was hyperopic, with a refractive error of +0.80D. When compared with the parameters used in the Bennetts and Rabbetts schematic eye, a 0.1-mm error in anterior corneal radius of curvature will cause 0.60D error in refraction; a 0.1-mm error in posterior corneal radius of curvature will cause 0.04D error in refraction; and a 0.1-mm error in corneal thickness will cause 0.025D error in refraction. These calculations show that, if uncorrected corneal parameters from raw AS-OCT images are used for refractive surgeries, CL fitting, or optical modeling, this would result in errors in refraction as high as 0.80D. The corrected corneal radii of curvature and thickness values obtained from the subjects are of a sufficiently high degree of accuracy to allow their use in future schematic eye calculations. The current study does not suggest that Visante should become a gold standard for corneal curvature measurements but simply demonstrates how the Visante can be used to extract accurate corneal radii of curvature values from human corneas.

CONCLUSIONS

This study demonstrates that spatial and optical distortions of the Visante AS-OCT measured front and back CL radii of curvatures can be corrected with a small residual error of 0.02 mm and 0.01 mm, respectively. Distorted and uncorrected corneal parameters can induce errors in ocular refraction as high as 0.80D. The Visante AS-OCT measured corneal parameters showed good intrasession and intersession repeatability. Corneal parameters from Visante AS-OCT after distortion corrections would be beneficial for future schematic eye calculations.

ACKNOWLEDGMENTS

The authors thank Dr. Jason Marsack, Jim Elswick, and Chris Kuether for technical assistance.

Received December 16, 2014; accepted July 2, 2015.

APPENDIX

The Appendix, a summary of the distortion correction method, is available at http://links.lww.com/OPX/A224.

REFERENCES

1. Dubbelman M, Sicam VA, van der Heijde GL. The shape of the anterior and posterior surface of the aging human cornea. Vision Res 2006;46:993–1001.
2. de Jong T, Sheehan MT, Dubbelman M, Koopmans SA, Jansonius NM. Shape of the anterior cornea: comparison of height data from 4 corneal topographers. J Cataract Refract Surg 2013;39:1570–80.
3. Dubbelman M, Weeber HA, van der Heijde RG, Volker-Dieben HJ. Radius and asphericity of the posterior corneal surface determined by corrected Scheimpflug photography. Acta Ophthalmol Scand 2002;80:379–83.
4. Liu Z, Huang AJ, Pflugfelder SC. Evaluation of corneal thickness and topography in normal eyes using the Orbscan corneal topography system. Br J Ophthalmol 1999;83:774–8.
5. Crawford AZ, Patel DV, McGhee CN. Comparison and repeatability of keratometric and corneal power measurements obtained by Orbscan II, Pentacam, and Galilei corneal tomography systems. Am J Ophthalmol 2013;156:53–60.
6. Zheng S, Ying J, Wang B, Xie Z, Huang X, Shi M. Three-dimensional model for human anterior corneal surface. J Biomed Opt 2013;18: 065002.
7. Al-Farhan HM, Al-Otaibi WM. Comparison of central corneal thickness measurements using ultrasound pachymetry, ultrasound biomicroscopy, and the Artemis-2 VHF scanner in normal eyes. Clin Ophthalmol 2012;6:1037–43.
8. Ogbuehi KC, Osuagwu UL. Repeatability and interobserver reproducibility of Artemis-2 high-frequency ultrasound in determination of human corneal thickness. Clin Ophthalmol 2012;6:761–9.
9. Fishman GR, Pons ME, Seedor JA, Liebmann JM, Ritch R. Assessment of central corneal thickness using optical coherence tomography. J Cataract Refract Surg 2005;31:707–11.
10. Zhao PS, Wong TY, Wong WL, Saw SM, Aung T. Comparison of central corneal thickness measurements by Visante anterior segment optical coherence tomography with ultrasound pachymetry. Am J Ophthalmol 2007;143:1047–9.
11. Sorbara L, Maram J, Fonn D, Woods C, Simpson T. Metrics of the normal cornea: anterior segment imaging with the Visante OCT. Clin Exp Optom 2010;93:150–6.
12. Ramasubramanian V, Glasser A. Prediction of accommodative optical response in prepresbyopic subjects using ultrasound biomicroscopy. J Cataract Refract Surg 2015;41:964–80.
13. Ramasubramanian V, Glasser A. Can ultrasound biomicroscopy be used to predict accommodation accurately? J Refract Surg 2015; 31:266–73.
14. Ramasubramanian V, Glasser A. Objective measurement of accommodative biometric changes using ultrasound biomicroscopy. J Cataract Refract Surg 2015;41:511–26.
15. Carl Zeiss Meditec. Visante OCT User Manual. Dublin, CA: Carl Zeiss Meditec, Inc.; 2006.
16. Westphal V, Rollins A, Radhakrishnan S, Izatt J. Correction of geometric and refractive image distortions in optical coherence tomography applying Fermat's principle. Opt Express 2002;10: 397–404.
17. Podoleanu A, Charalambous I, Plesea L, Dogariu A, Rosen R. Correction of distortions in optical coherence tomography imaging of the eye. Phys Med Biol 2004;49:1277–94.
18. Borja D, Siedlecki D, de Castro A, Uhlhorn S, Ortiz S, Arrieta E, Parel JM, Marcos S, Manns F. Distortions of the posterior surface in optical coherence tomography images of the isolated crystalline lens: effect of the lens index gradient. Biomed Opt Express 2010; 1:1331–40.

19. Siedlecki D, de Castro A, Gambra E, Ortiz S, Borja D, Uhlhorn S, Manns F, Marcos S, Parel JM. Distortion correction of OCT images of the crystalline lens: gradient index approach. Optom Vis Sci 2012; 89:E709–18.
20. Dunne MC, Davies LN, Wolffsohn JS. Accuracy of cornea and lens biometry using anterior segment optical coherence tomography. J Biomed Opt 2007;12:064023.
21. Kao CY, Richdale K, Sinnott LT, Grillott LE, Bailey MD. Semi-automatic extraction algorithm for images of the ciliary muscle. Optom Vis Sci 2011;88:275–89.
22. Kasarova SN, Sultanova NG, Ivanov CD, Nikolov ID. Analysis of the dispersion of optical plastic materials. Opt Mater 2007;29: 1481–90.
23. Yuen LH, He M, Aung T, Htoon HM, Tan DT, Mehta JS. Biometry of the cornea and anterior chamber in chinese eyes: an anterior segment optical coherence tomography study. Invest Ophthalmol Vis Sci 2010;51:3433–40.
24. Tan DK, Chong W, Tay WT, Yuen LH, He M, Aung T, Tan DT, Wong TY, Mehta JS. Anterior chamber dimensions and posterior corneal arc length in Malay eyes: an anterior segment optical coherence tomography study. Invest Ophthalmol Vis Sci 2012;53: 4860–7.
25. Chen MJ, Liu YT, Tsai CC, Chen YC, Chou CK, Lee SM. Relationship between central corneal thickness, refractive error, corneal curvature, anterior chamber depth and axial length. J Chin Med Assoc 2009;72:133–7.
26. Rufer F, Schroder A, Bader C, Erb C. Age-related changes in central and peripheral corneal thickness: determination of normal values with the Orbscan II topography system. Cornea 2007;26:1–5.
27. Hashemi H, Yazdani K, Mehravaran S, Khabazkhoob M, Mohammad K, Parsafar H, Fotouhi A. Corneal thickness in a population-based, cross-sectional study: the Tehran Eye Study. Cornea 2009;28:395–400.
28. Doughty MJ, Zaman ML. Human corneal thickness and its impact on intraocular pressure measures: a review and meta-analysis approach. Surv Ophthalmol 2000;44:367–408.
29. Siu A, Herse P. The effect of age on human corneal thickness. Statistical implications of power analysis. Acta Ophthalmol (Copenh) 1993;71:51–6.
30. Galgauskas S, Norvydaite D, Krasauskaite D, Stech S, Asoklis RS. Age-related changes in corneal thickness and endothelial characteristics. Clin Interv Aging 2013;8:1445–50.
31. Aghaian E, Choe JE, Lin S, Stamper RL. Central corneal thickness of Caucasians, Chinese, Hispanics, Filipinos, African Americans, and Japanese in a glaucoma clinic. Ophthalmology 2004;111:2211–9.
32. Li H, Leung CK, Wong L, Cheung CY, Pang CP, Weinreb RN, Lam DS. Comparative study of central corneal thickness measurement with slit-lamp optical coherence tomography and Visante optical coherence tomography. Ophthalmology 2008;115:796–801.
33. Savini G, Barboni P, Carbonelli M, Hoffer KJ. Repeatability of automatic measurements by a new Scheimpflug camera combined with Placido topography. J Cataract Refract Surg 2011;37:1809–16.
34. Huang J, Savini G, Wang C, Lu W, Gao R, Li Y, Wang Q, Zhao Y. Precision of corneal thickness measurements obtained using the Scheimpflug-Placido imaging and agreement with ultrasound pachymetry. J Ophthalmol 2015;2015:328798.
35. Hernandez-Camarena JC, Chirinos-Saldana P, Navas A, Ramirez-Miranda A, de la Mota A, Jimenez-Corona A, Graue-Hernindez EO. Repeatability, reproducibility, and agreement between three different Scheimpflug systems in measuring corneal and anterior segment biometry. J Refract Surg 2014;30:616–21.
36. Bennett AG, Rabbetts RB. The schematic eye. In: Rabbetts RB, ed. Bennett & Rabbetts' Clinical Visual Optics, 4th ed. Philadephia, PA: Elsevier/Butterworth-Heinemann; 2007;221–43.

Adrian Glasser
College of Optometry
University of Houston
4901 Calhoun Rd
Houston, TX 77204
e-mail: aglasser@uh.edu

Appendix

Summary of the Distortion Correction Method

The corneal surface coordinates are converted from pixels to mm and scaled such that vertex is at x = 0, y = 0. Distortion correction equations are used in the order listed to correct distortions of corneal parameters. x_a, y_a and x_p, y_p: x and y coordinates of the circle fits to the anterior and posterior corneal surface, respectively; F: surface power of the anterior cornea; L and L' : object and image vergence at the actual and optically distorted posterior corneal surfaces, respectively; CT_{OCT} : corneal thickness measured from OCT image; $Corr\_CT$: optically corrected corneal thickness; L_2 and L_2' : object and image vergence at the spatial and optical distortion corrected posterior corneal surface center of curvatures, respectively; $Corr\_r_{PC}$: optically corrected posterior corneal radius of curvature; n_{cornea}: refractive index of cornea for AS-OCT wavelength of 1310 nm was calculated to 1.4015 using the equation[32] $n_{cornea} = 1.376 + 0.0512 - (0.1455 \times 1.310) + 0.0961 \times 1.310^2$.

ANTERIOR CORNEAL SURFACE

Spatial distortion correction

a) $y_a = -8.77696399112472e^{-8} \times x_a^6 - 1.26047098634593e^{-10} \times x_a^5 - 1.7111029593407e^{-6} \times x_a^4 + 1.87608071693789e^{-9} \times x_a^3 - 1.0224453717464e^{-4} \times x_a^2 - 5.1881743271264e^{-9} \times x_a + 1.00000075090351$ ------ (1)

b) Calculate the anterior corneal radius of curvature (r_{AC}) from the coordinates x_a and y_a.

c) Apply a second step of correction to get spatial distortion corrected radius ($Corr\_r_{AC}$).

$Corr_{r_{AC}} = -0.0981 \times (r_{AC})^2 + (2.4408 \times r_{AC}) - 5.2593$ ------ (2)

CENTRAL CORNEAL THICKNESS

Optical distortion correction

a) $F = \frac{1000 \times (n_{cornea} - 1)}{Corr\_r_{AC}}$ ------ (3)

b) $L' = \frac{1000 \times n_{cornea}}{CT_{OCT}}$ ------ (4)

c) $L = L' - F$ ------ (5)

d) $Corr\_CT = \frac{1000}{L}$ ------ (6)

POSTERIOR CORNEAL SURFACE

Spatial distortion correction

a) $y_p = -7.94584588229656e^{-7} \times x_p^6 + 4.06594066225371e^{-9} \times x_p^5 - 1.3899072311646907e^{-5} \times x_p^4 - 6.05389906276954e^{-8} \times x_p^3 - 8.19165078653822e^{-4} \times x_p^2 + 1.66111950474094e^{-7} \times x_p + 1.00000708889656$ ------ (7)

b) Calculate the posterior corneal radius of curvature (r_{PC}) from the coordinates x_p and y_p.

c) Apply a second step of correction to get spatial distortion corrected radius ($SCorr\_r_{PC}$).

$SCorr_{r_{PC}} = -0.0323 \times (r_{PC})^2 + (1.8024 \times r_{PC}) - 4.0057$ ------ (8)

Optical distortion correction

a) $L_2 = \frac{1000}{SCorr_{r_{PC}} + CT_{OCT}}$ ------ (9)

b) $L_2' = L_2 + F$ ------ (10)

c) $Corr\_r_{PC} = \frac{1000 \times n_{cornea}}{L_2'} - Corr\_CT$ ------ (11)